Parametric Study by Design of Experiments of Thermal Management of a Light-Emitting Diode Dissipator in a Cavity

Zouhour Araoud, Khaoula Ben Abdelmlek, Kamel Charrada, Georges Zissis, Laurent Canale

Parametric Study by Design of Experiments of Thermal Management of a Light-Emitting Diode Dissipator in a Cavity

Zouhour Araoud [1,*], Khaoula Ben Abdelmlek [2], Kamel Charrada [2], Georges Zissis [3] and Laurent Canale [3,*]

[1] Laboratoire EMIR, ENIM, Université de Monastir, Monastir LR20ES08, Tunisia
[2] Laboratoire EMIR, IPEIM, Université de Monastir, Monastir LR20ES08, Tunisia; khaoula.benabdelmlek@ipeim.rnu.tn (K.B.A.); kamel.charrada@ipeim.rnu.tn (K.C.)
[3] LAPLACE, Université de Toulouse, CNRS, INPT, UPS, Toulouse, France; georges.zissis@laplace.univ-tlse.fr
* Correspondence: zouhour.ara@enim.rnu.tn (Z.A.); laurent.canale@laplace.univ-tlse.fr (L.C.)

Abstract: This paper presents the results of a numerical investigation by design of experiments of the thermal management of a symmetrical rectangular heat sink for LED lighting placed in a cavity with asymmetrical conditions at its opening. Our mathematical model is validated by an experiment we carried out for an LED placed in a cavity. According to the proposed design of experiments (2^4 factorial designs), we analyzed, by simulation modeling using COMSOL Multiphysics®, the influence of the different controllable parameters (the position A and width C of the openings, the inlet air velocity B, and the cavity height D) on the evolution of the junction temperature in order to optimize the thermal management of the proposed LED lamp. Using Minitab® manipulation software, a Pareto analysis and an analysis of variance (ANOVA) were carried out, and mathematical models were deduced to estimate the optimal junction temperature and the convective heat transfer coefficient of the proposed radiator and the surrounding air as a function of the controlled parameters. It was found that the position of the opening is the most influential factor on the junction temperature, with a contribution of 93.46%, followed by the factors velocity and width of the opening, with low contributions (3.22% and 1.24%). We also observe that the height of the cavity and the interactions (A × C, A × D, B × C, B × D, C × D) have no significant influence on the junction temperature.

Keywords: heat transfer; convective heat transfer rate; partially opened cavity; design of experiments

1. Introduction

High-power white LEDs are anticipated to last for a very long time—in the range of several tens of thousands of hours [1–5]. Though they typically do not fail completely, LEDs gradually lose some of their light intensity over time [6]. A study of the lifetime of a white LED as a function of junction temperature was reported by Wang and Lu [7]. The findings unequivocally demonstrate that prolonging the lifespan of light-emitting diodes requires lowering the diode junction temperature, which can be accomplished through effective thermal management. For some lighting applications, that occasionally requires that the heat sink for the LED lamp be fitted into a tight area, like a false or slanted ceiling, and the issue only grows worse over time since the amount of heat that can be transferred outside is restricted.

The symmetrical situation of cooling heat sinks in open space has received the majority of attention in earlier works [8–19]. However, despite its significant impact on the performance of LED lamps, the situation of cooling the heat sink in enclosures is less considered. Actually, research on natural convection heat transfer in enclosures was done for uses involving electronic cooling. The shape, size, and orientation of the cavity are significant factors that influence the amount of heat evacuated, according to previous numerical studies [20–23].

Nada's experimental work [20] focuses on the investigation of natural convection in a cavity holding a rectangular heat sink with fins. The authors next came up with an ideal fin spacing that optimizes both the rate of heat transfer and the effectiveness of the fins.

In [21–23], the authors examined a natural convection scenario involving a rectangular finned heat sink positioned inside a rectangular cavity. It was considered that the cavity's lateral sides are adiabatic; the upper side is maintained at a cold temperature, while the lower side is kept at a hot temperature. Both the length and the spacing of the fins have been examined for their effects. Hasnaoui et al. [23] used numerical analysis to resolve the Navier–Stokes equations in their dimensionless form in order to study the same setup with adiabatic fins. They discovered that the cavity aspect ratio, cooling ribs length, fin aspect ratio (the fin length vs spacing between them), and the cavity inclination are the variables influencing the heat transfer rate. In our recent article [24], we looked at how the cavity's length and orientation affected the thermal and optical characteristics of the LED device. We discovered that the ideal cavity length for maximizing heat transmission in the cavity is four times the length of the heat sink fins.

Because of the relatively low heat transfer coefficient during passive cooling, a larger heat transfer area than during active cooling is needed to dissipate the same quantity of heat at the same temperature difference [25]. The benefits of passive cooling include zero energy usage, quiet operation, and high reliability because there are no moving parts. Large, heavy heat sinks and the inability to regulate the heat transfer rate are drawbacks. Therefore, natural convection cannot maintain the LED junction temperature at a constant level under changing ambient temperature circumstances or varying heat generation. Since forced convection accounts for the majority of active cooling, its heat transfer coefficient is much greater than that of natural convection. With the same heat flow rate from the heat source and the same temperature differential, this enables a smaller heat transfer area of the heat sink than would be the case naturally. The benefit of active cooling is the ability to regulate the heat flow rate in order to maintain a consistent LED junction temperature regardless of changes in the ambient temperature.

In this context, we propose an asymmetrical model that consists of creating openings on the sidewalls of the cavity, where a heat sink is located, and studying the influence of the different controllable parameters in the case of forced convection (the position and width of the openings, the cavity height, and the air velocity) on the evolution of the junction temperature and the convective heat transfer coefficient in order to boost the heat transfer and increase the lifespan of the LED lamp. Our three-dimensional simulation models have many input parameters, and predicting which ones have a significant influence on junction temperature can be a challenge. The most common method is to modulate one parameter at a time, but 1/ this is very inefficient and time-consuming, and 2/ more seriously, this method can be wrong because in many cases, the different factors can interact and produce a response induced by the simultaneous action of several factors [26–30]. In this paper, we use a full factorial design of experiments whose major goal is to calculate the important factors and mathematical correlations to determine the junction temperature and the convective heat coefficient of air around the proposed heat sink.

2. Problem Formulation and Numerical Methodology

From the reference configuration (Figure 1), three-dimensional modeling was carried out in a Cartesian coordinate system.

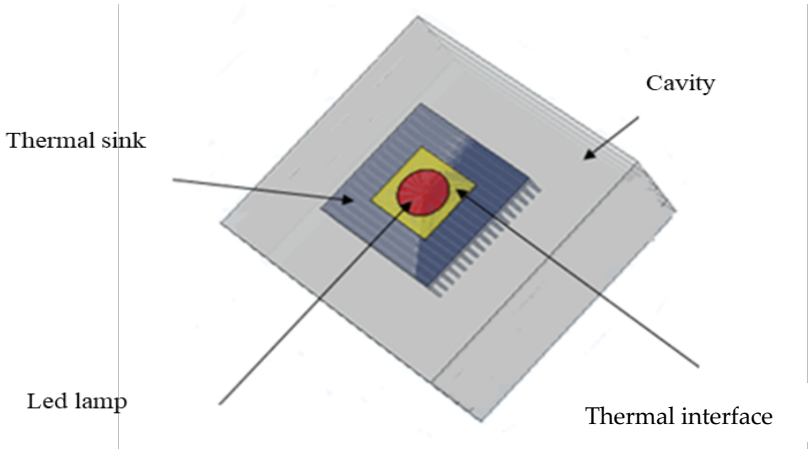

Figure 1. Different components of the model.

The system consists of several components designed for effective thermal management of the LED. The LED chip is made of gallium nitride (GaN), selected for its excellent light emission properties and high thermal stability under elevated temperatures [31]. Furthermore, these nitride LED materials are also simulated for these properties by phase field models combined with a Density Functional Theory–Fed Phase Field Model [32]. A thermal interface material (TIM), composed of a graphite interface, is used to improve the thermal contact between the LED chip and the substrate. The substrate is made of copper, chosen for its high thermal conductivity, which efficiently transfers heat from the LED chip to the heat sink. The heat sink is constructed from aluminum, known for its good thermal conductivity, light weight, and cost-effectiveness in dissipating heat into the surrounding environment.

2.1. Geometry and Thermal Characteristics of Different Parts of the System

The thermal characteristics of the different elements of the luminaire, as well as its dimensions, are presented in Table 1 below. The study is based on a relatively common heat sink, comprising a variable number of fins (17 fins) and length H. Each of the fins (of a constant thickness, e = 0.2 cm) is spaced by a distance d (0.61 cm).

Table 1. Thermal characteristics and geometric dimensions of the different elements of the luminaire.

Component	Dimensions	Material	k (W/m·K)	Cp (J/kg·K)	ϱ (kg/m³)	μ (Pa·s)
LED chip	Diameter: 3.5 cm Height: 0.17 cm	GaN	k_L (T)	C_{pL} (T)	ϱ_L (T)	N.U.
Thermal paste TIM	d = 50 μm	Thermal grease	3	1200	N.U.	N.U.
Substrate	5.08 cm × 5.08 cm × 0.17 cm	Copper	400	385	8960	N.U.
Heat sink	10 cm ×10 cm × 2.5 cm	Aluminum	238	900	2700	N.U.
Cavity	20 cm × 25 cm × 10 cm	Air	k_a (T)	C_{pa} (T)	ϱ_a (T)	μa (T)

N.U.: not used.

k_L and k_a are the thermal conductivity of the LED chip and the air, respectively, calculated using the following equation, and the different coefficients a_{ik} are given in Table 2.

$$k(T) = \sum_{i=0}^{5} a_{ik}\, T^i \quad (1)$$

Table 2. Coefficients related to the thermal conductivity.

	LED Chip	Air
a_{0k}	0.385376404	−0.00227583562
a_{1k}	0.155494059	1.15480022E-4
a_{2k}	−0.00389712867	−7.90252856E-8
a_{3k}	7.42125697E-5	4.11702505E-11
a_{4k}	−7.10185482E-7	−7.43864331E-15
a_{5k}	2.58023057E-9	0

The specific heat is calculated using Equation (2), and the different coefficients are given in Table 3.

$$C_p(T) = \sum_{i=0}^{4} a_{Ci}\, T^i \quad (2)$$

Table 3. Coefficients related to the specific heat.

	LED Chip	Air
a_{C0}	350.886683	1047.63657
a_{C1}	0.467877892	−0.372589265
a_{C2}	−1.40291068E-4	9.45304214E-4
a_{C3}	0	−6.02409443E-7
a_{C4}	0	1.2858961E-10

The LED chip density ϱ_L is calculated using Equation (3). The coefficients a_{Li} are given in Table 4.

$$\rho_L(T) = \sum_{i=0}^{3} a_{Li}\, T^i \quad (3)$$

Table 4. Coefficients related to the density of the LED chip.

a_{L0}	a_{L1}	a_{L2}	a_{L3}
7576.346	−0.485959	2.27453E-6	−1.62125E-7

The dynamic viscosity of the air is calculated using Equation (4). The coefficients a_{ai} are given in Table 5.

$$\mu_a(T) = \sum_{i=0}^{4} a_{ai}\, T^i \quad (4)$$

Table 5. Coefficients related to the density of the LED chip.

a_{a0}	a_{a1}	a_{a2}	a_{a3}	a_{a4}
−8.38E-7	8.357172E-8	−7.6942E-11	4.643E-14	1.06585E-17

ϱ_a is the air density, which is calculated from the ideal gas law:

$$\rho_a = \frac{P_{atm}}{\left(R/M_w\right) T} \quad (5)$$

where $M_w = 28.97$ kg/kmol, is the molecular weight of air.

2.2. Initial Hypotheses and Basic Theoretical Equations

The following assumptions are made as a starting point:

- The airflow is incompressible, laminar, and Newtonian (constant viscosity).
- All the constituent materials of the system (heat sink, LED, etc.) are homogeneous and isotropic.
- The thermal characteristics of the different materials (except air and the LED light source) are assumed to be independent of temperature and constant [33].

With these basic principles, the relationships that govern the studied device are as follows.

For the air side

Continuity

$$\frac{\partial(\rho u)}{\partial x} + \frac{\partial(\rho v)}{\partial y} + \frac{\partial(\rho w)}{\partial z} = 0 \quad (6)$$

Momentum equations in 3D dimensions (x, y and z):

$$\frac{\partial \rho u}{\partial t} + \frac{\partial(\rho u^2)}{\partial x} + \frac{\partial(\rho uv)}{\partial y} + \frac{\partial(\rho uw)}{\partial z} = -\frac{\partial P}{\partial x} + \mu\left(\frac{\partial^2 u}{\partial x^2} + \frac{\partial^2 u}{\partial y^2} + \frac{\partial^2 u}{\partial z^2}\right) \quad (7)$$

$$\frac{\partial \rho v}{\partial t} + \frac{\partial(\rho uv)}{\partial x} + \frac{\partial(\rho v^2)}{\partial y} + \frac{\partial(\rho vw)}{\partial z} = -\frac{\partial P}{\partial y} + \mu\left(\frac{\partial^2 v}{\partial x^2} + \frac{\partial^2 v}{\partial y^2} + \frac{\partial^2 v}{\partial z^2}\right) \quad (8)$$

$$\frac{\partial \rho w}{\partial t} + \frac{\partial(\rho uw)}{\partial x} + \frac{\partial(\rho vw)}{\partial y} + \frac{\partial(\rho w2)}{\partial z} = -\frac{\partial P}{\partial z} + \mu\left(\frac{\partial^2 w}{\partial x^2} + \frac{\partial^2 w}{\partial y^2} + \frac{\partial^2 w}{\partial z^2}\right) - \rho g \quad (9)$$

Energy equation

$$\frac{\partial(\rho uT)}{\partial x} + \frac{\partial(\rho vT)}{\partial y} + \frac{\partial(\rho wT)}{\partial z} = \frac{k}{C_p}\left(\frac{\partial^2 T}{\partial x^2} + \frac{\partial^2 T}{\partial y^2} + \frac{\partial^2 T}{\partial z^2}\right) \quad (10)$$

And the energy equation for the solid side:

$$\rho C_p \frac{\partial T}{\partial t} = k\left(\frac{\partial^2}{\partial x^2}T + \frac{\partial^2}{\partial y^2}T + \frac{\partial^2}{\partial z^2}T\right) \quad (11)$$

where C_p is the specific heat;

μ, the dynamic viscosity;

ρ, the density;

g, the gravity acceleration;

k, the thermal conductivity;

T, the temperature;

t, the time;

p, the pressure;

and u, v and w are the velocity components in the x, y and z directions, respectively.

2.3. Boundary Conditions of the System Studied

These conditions are symmetrical and correlated with the equations as follows:

- The injected power of the LED light source is equal to 36.3 W. The efficiency of an LED light source is in the order of 30%, and there is no loss other than thermal losses. So, 70% of the injected power is converted into heat [34–36]. The dissipated power Φ is then equal to 25.41 W.
- We consider the following boundary condition: the heat flow on the base of the heat sink is uniform:

$$u = v = w = 0;\ -\mathrm{ks}\ \partial \mathrm{T}/\partial \mathrm{n}\ =\ \Phi \quad (12)$$

where n is the normal distance to the surface of the baseboard.

- All the sidewalls of the cavity except the openings are maintained adiabatic.

$$u = v = w = 0; \partial \mathrm{T}/\,\partial \mathrm{n} \;=\; 0 \tag{13}$$

- We consider a conjugate heat transfer at the interface between solid and fluid. We have applied to our study these conditions between the air (fluid) and the heat sink (solid), and then, the heat transfer inside the aluminum basement (solid) follows the Laplace equation, and the one inside the air (fluid), the Navier–Stokes equation. Considering the continuity between the aluminum and the air (solid and fluid domains), solving this equation system allows us to determine the temperature and heat flux distributions on this interface.

The following equations govern the continuity condition between the heat sink and the air:

$$\mathrm{T}_{\mathrm{fluid,\ interface}} = \mathrm{T}_{\mathrm{solid,\ interface}}$$

$$k_{fluid} \left.\frac{\partial T_{fluid}}{\partial n}\right|_{interface} = k_{solid} \left.\frac{\partial T_{solid}}{\partial n}\right|_{interface} \tag{14}$$

2.4. Mesh and Simulation

The numerical simulation was conducted using COMSOL Multiphysics®, a commercial code based on the finite element method. We chose to work with a normal mesh composed of 760841 domain elements, 58744 boundary elements, and 5246 edge elements. It was found that additional elements had no effect on the temperature variation.

The temperature distribution and the velocity vectors inside the cavity are presented in Figure 2. We notice that there is a profile of symmetry with respect to the median vertical of the cavity: the direction of the airflow is from the bottom, at the level of the LED (heat source) towards the top (the heat sink), then it rises until it reaches the upper wall of the cavity, then the air follows the shape of the cavity and ends up going down the sidewalls. At this stage, we witness the formation of boundary layers that play an important role in cooling the hot air coming from the LED.

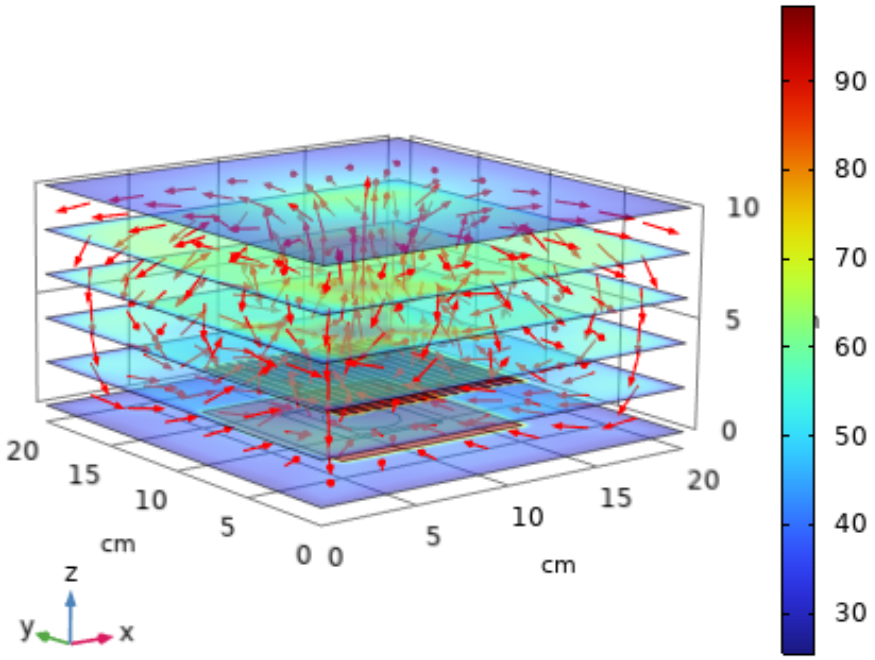

(**a**)

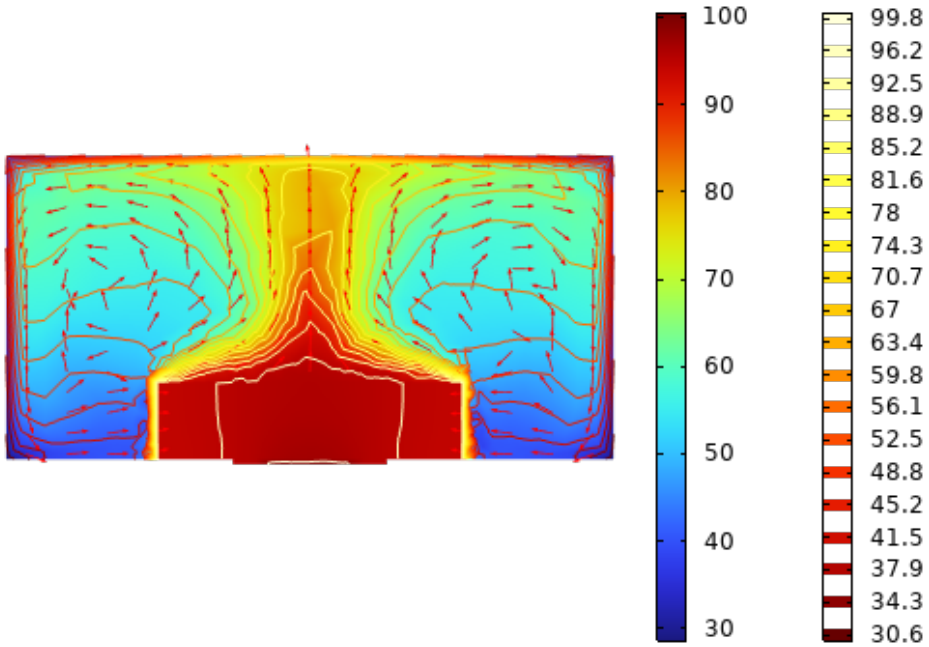

(**b**)

Figure 2. Symmetrical temperature and velocity fields at t = 2500 s; (**a**) in 3D presentation; (**b**) in 2D presentation (y-z cut plane, x = 10 cm).

3. Experiment and Model Verification

In order to validate the simulation, from the results found with COMSOL Multiphysics®, an experiment was carried out and the results obtained were compared with the numerical ones.

3.1. Presentation of the Experiment

To carry out the experiment, we used an LED of type BXTRA-W3500 and an aluminum heat sink with the same dimensions and properties given in Table 1. Temperature measurements were conducted using Type K thermocouples (temperature range 0–1100 °C), positioned as shown in Figure 3, to record temperatures over time at specific points on the LED and the heat sink. These thermocouples were connected to a PicoLog (TC-08) data logging station, linked to a computer for real-time display and recording of temperature profiles. The system was powered using a voltage generator (U = 22 V and I = 1.65 A) and placed in a cavity open on two sides, where the external temperature was maintained at 22 °C (measured with a fifth thermocouple). To minimize external disturbances, the entire setup was enclosed in a large box, as shown in Figure 4.

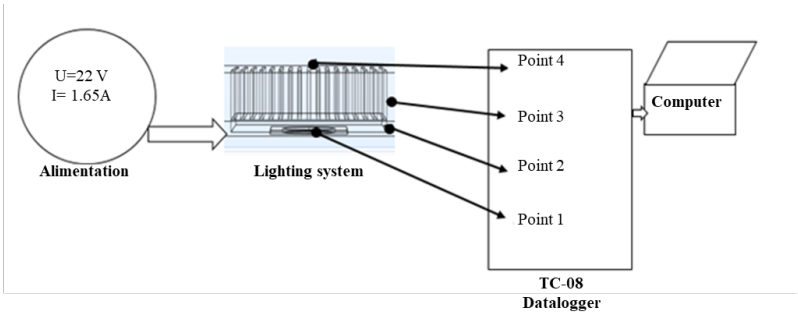

Figure 3. Simplified measurements setup diagram.

Figure 4. Experimental setup.

3.2. Data Acquisition and Processing

To ensure accurate and reliable results, the temperature sampling rate was set to 1 Hz, meaning that one measurement was taken every second at four specific points. At each time step, three samples were taken at each measurement point. These samples were then averaged to reduce measurement noise and ensure data reliability. The entire experiment was repeated three times under identical conditions to verify the overall consistency and robustness of the data.

To assess the uncertainty of the results, several sources of uncertainty were considered: the Type K thermocouple, classified under class 1 tolerance, has a tolerance limit of ±1.5 °C; the PicoLog TC-08 has a tolerance of ±0.5 °C; and cold junction compensation introduces an additional uncertainty of approximately ±0.5 °C. By combining these uncertainties using the root–sum–square (RSS) method, the overall uncertainty was estimated to be approximately ±1.65 °C. These considerations were carefully integrated into the analysis to ensure the reliability of the numerical validation.

3.3. Validation

In order to make a comparison between the experimental and the numerical results, we plotted, as shown in Figure 5, curves of the evolution of temperature as a function of time at the level of each point shown in Figure 6. The experimental measurements and the model present a very good correlation, which validates the numerical model.

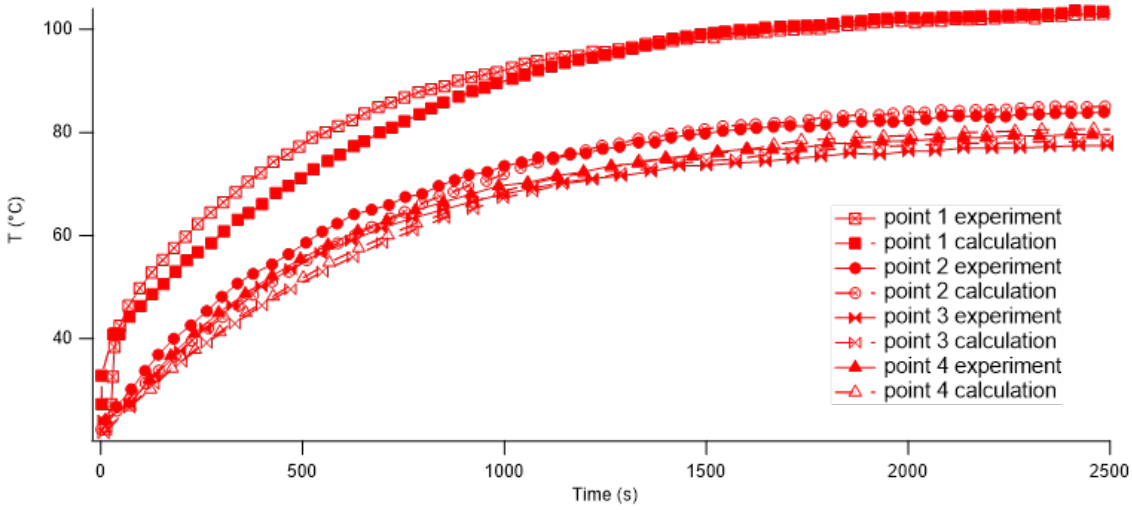

Figure 5. Numerical and experimental measurements of the temperature at different points.

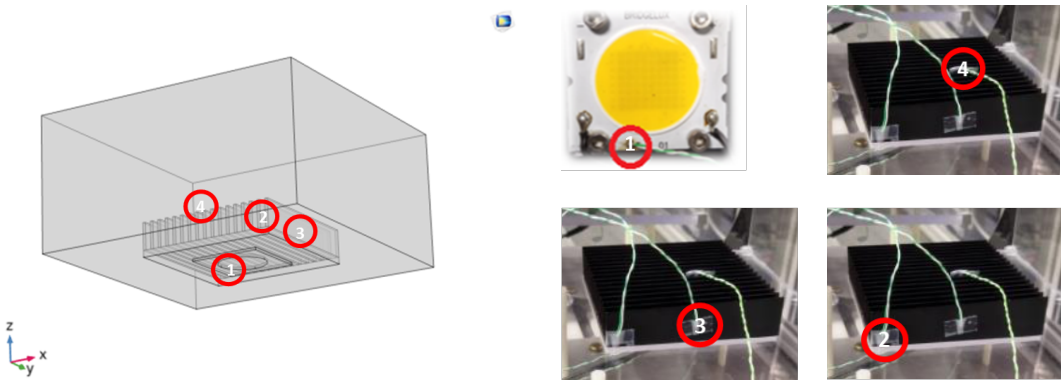

(**a**) (**b**)

Figure 6. The different points chosen for the numerical study (**a**) and experiment (**b**)—Point 01: at the LED—Point 02: between two fins—Point 03: at the level of the heat sink base—Point 04: at the level of the fin.

4. Results

4.1. Design of Experiments (DoE): A Parametric Study

The position (A) and the width (C) of the openings, and the height of the cavity (D) as well as the air velocity (B) are the main parameters influencing the junction temperature (Tj), as presented in Figure 7. Table 6 gives their levels of influence in their reduced and real values.

Table 6. Main factors and their corresponding levels of influence.

Factors	Level	
	Reduced Value	Real Value
Position (A)	−1	0 cm
	+1	5 cm
Velocity (B)	−1	1 m/s
	+1	2 m/s
Opening width (C)	−1	5 cm
	+1	10 cm
Cavity height (D)	−1	10 cm
	+1	20 cm

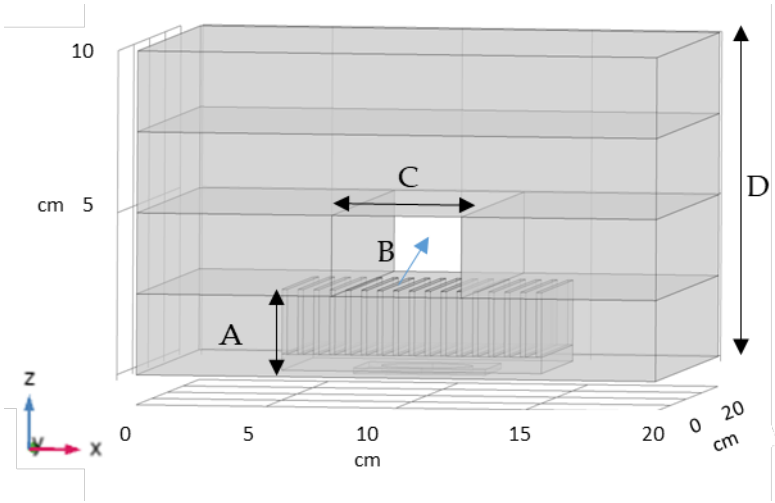

Figure 7. Geometry with holed cavity.

4.1.1. Design of Experiments

We consider a design of experiments composed of four factors at two levels, which results in a total number of trials equal to 16. Since this number is acceptable to work with, a complete factorial design was used according to which the experimental design matrix was given by Minitab® software and is presented in Table 7.

Table 7. Experimental design matrix.

Run N°	Experimental Factor Level				Response (°C)
	A	B	C	D	Tj
1	−1	−1	−1	+1	55.11
2	−1	−1	+1	−1	45.88
3	+1	−1	+1	+1	88.25
4	−1	+1	−1	+1	38.91
5	+1	−1	−1	−1	91.70
6	+1	+1	−1	+1	89.33
7	−1	+1	−1	−1	39.14
8	−1	−1	−1	−1	54.84
9	−1	−1	+1	+1	44.63
10	+1	−1	−1	+1	89.06
11	+1	+1	+1	+1	83.21
12	+1	+1	+1	−1	85.64
13	−1	+1	+1	+1	32.86
14	+1	−1	+1	−1	92.72
15	−1	+1	+1	−1	33.98
16	+1	+1	−1	−1	91.23

The computed temperatures vary between 32.86 °C and 92.72 °C. These values were obtained under different parameter settings and represent the expected thermal behavior of the system under realistic operating conditions. The highest calculated temperature, 92.72 °C, is well below the critical threshold of 120 °C, which is commonly accepted as the upper limit for safe LED operation. As such, the temperature range observed in our simulations confirms that the LED operates within a safe and optimal thermal range, preventing the risk of overheating and ensuring long-term performance and reliability.

4.1.2. Effects Study

Among the results obtained in Table 7, we could identify, using Minitab software, the most important effects in the formulation.

These effects are mentioned as statistically significant if the *p*-value mentioned in Table 8 is less than 0.05 and if our value of R^2 (the correlation coefficient) is close to 100%.

The *p*-value varies from 0 to 1 and expresses the probability that the results observed within a study can occur randomly:

- If $p > 0.05$, the factor is insignificant.
- If $p < 0.05$, the factor is significant.

It is clear in this table that the factor A, the position of the opening in the cavity, has the most influence on the temperature result Tj (°C) with the greatest effect (45.724).

Table 8. Effect matrix.

Term	Effect	Coeff.	*p*-Value
Constant		66.031	0.000
A	45.724	22.862	0.000
B	−8.486	−4.243	0.001
C	−5.269	−2.634	0.006
D	−1.721	−0.861	0.193
A × B	5.406	2.703	0.005
A × C	2.394	1.197	0.091
A × D	−1.139	−0.569	0.366
B × C	−0.461	−0.231	0.704
B × D	0.301	0.151	0.803
C × D	−0.596	−0.298	0.625

4.1.3. Regression Equation

To enhance clarity and focus on significant effects, we repeated the iteration while eliminating statistically insignificant components (D, AC, AD, BC, BD, CD) from our model and identified a reduced model that includes only significant factors (A, B, AB, C). This adjustment allowed us to present a clearer analysis of the results.

The regression equation reveals the combination between the junction temperature (Tj) and the other independent variables studied (the position of the opening (A), its width (C), and the air inlet velocity (B) are given in Equation (15)). The temperature is expressed by the quadratic mathematical model, and the values of the correlation coefficients are given in Table 9.

$$Tj\ (°C) = a_0\ + a_1 \times A + \ a_2 \times \ B + a_3 \times \ C + \ a_{12} \ \times \ A \times B \quad (15)$$

Table 9. Correlation coefficients.

a_0	a_1	a_2	a_3	a_{12}
66.031	22.862	− 4.243	− 2.634	2.703

The intercept (66.031 °C) represents the baseline temperature when all factors are at their reference levels, typically the center or average values of each factor's range. The main effects show that position has a positive relationship with temperature, meaning that an increase in position leads to a rise in temperature by 22.862 °C, assuming the other factors are constant. In contrast, velocity has a negative effect, with each unit increase in velocity resulting in a decrease in temperature by 4.243 °C. Similarly, increasing the opening width decreases the temperature by 2.634 °C. There is also an interaction between

position and velocity, with a positive coefficient of 2.703, meaning that the effect of position on temperature becomes more significant at higher velocities, and vice versa.

The model summary given in Table 10 indicates that the model fits the data very well. The standard error **S** suggests that, on average, the predictions made by the model are off by about **2.5 °C** from the actual temperature values, which is relatively small, indicating good precision. The coefficient of determination R^2 = 99.23%, which indicates that the modeling is suitable since this coefficient is very close to 1. In fact, this value can only explain 99.23% of the variability in the response by the model, and, therefore, 0.77% remains unexplained. This value of the coefficient of determination indicates that the junction temperature measurements obtained are modeled very satisfactorily by the model. This coefficient is adjusted to reach R^2(adj) = 98.95%. This correction of the R^2 allows us to take into account the number of parameters used in our model. Additionally, the predicted R^2 (R^2(pred)) is also high, which indicates that the model will likely perform well on other new data cases. These coefficients indicate a good correlation and a qualitative agreement between the model and the data.

Table 10. Model summary for the reduced model.

S	R^2	R^2(adj)	R^2(pred)
2.50	99.23%	98.95%	98.37%

5. Discussion

5.1. Statistical Analysis

5.1.1. Analysis of Variance (ANOVA)

The ANOVA is useful for studying the influence of input variables from the results obtained, while using the experimental design method. Moreover, it allows us to present an interpretation of the results (output data). It is based on the partition of the total variation in the modeling into elements attributed to the controlled parameters and the errors made.

Equation (16) expresses the sum of squares (SC) to estimate the square deviation from the overall mean.

$$SC_f = \frac{N}{N_{nf}} \sum_{i=1}^{N_{nf}} (\overline{y_i} - \overline{y})^2 \quad (16)$$

With $\overline{y} = \frac{1}{N} \sum_{i=1}^{N} y_i$, average responses include the following:

y_i: mean response observed in the modeling;

N: total number of modeling;

N_{nf}: factor level.

The mean of squares (MC) is calculated by dividing the sum of squares SS by the degree of freedom df_i.

$$MC_i = \frac{SS}{df_i} \quad (17)$$

Then, we calculate the contribution of each factor to the total variation, the last column of the ANOVA table (cont.%), to show the influence on the result.

$$\text{Cont.\%} = \frac{SC_f}{SC_T} \text{x} 100 \quad (18)$$

Table 11 shows the ANOVA results for the LED lamp junction temperature corresponding to the reduced model. The goal is to analyze the effects of the main factors as well as their interactions on (Tj).

Table 11. ANOVA results for junction temperature for the reduced model.

Source	DF	Adj SS	Adj MS	F-Value	*p*-Value	Cont.%
A: Opening position	1	8362.65	8362.65	1592.42	0.000	93.46%
B: Air velocity	1	288.07	288.07	54.85	0.001	3.22%
A × B	1	116.91	116.91	22.26	0.005	1.30%
C: Opening width	1	111.04	111.04	21.14	0.006	1.24%
Error	11	68.85				0.78%
Total	15	8947.51				100%

The Fisher's F test for our model was calculated with Minitab® software (F-value = 169.88), and the probability associated with the Fisher test (F-value) is equal to 0. This shows that the risk of the model being insignificant is 0%. In conclusion, ANOVA makes it possible to qualify the selected model.

In Table 11, it is clear that A, the position of the opening, is the most influential factor on the temperature (Tj), with a contribution of 93.46%. This shows that the positioning of the opening is crucial for heat dissipation, as it directly affects airflow. The air velocity (B) also plays a moderately important role, contributing 3.22% to the temperature variation. Faster airflow helps to carry heat away more efficiently, although its impact is much smaller compared to the opening position. The opening width (C**)** has a smaller effect, with just 1.24% of the variation explained. Lastly, the A × B interaction (1.30%) shows that the combined effect of the opening position and air velocity is important, showing that airflow works best when paired with an optimal opening position.

5.1.2. Pareto Chart and Graphical Analysis of the Results Obtained

The Pareto chart below (Figure 8) gives the importance of the influence of each parameter estimated for the reduced model, in descending order.

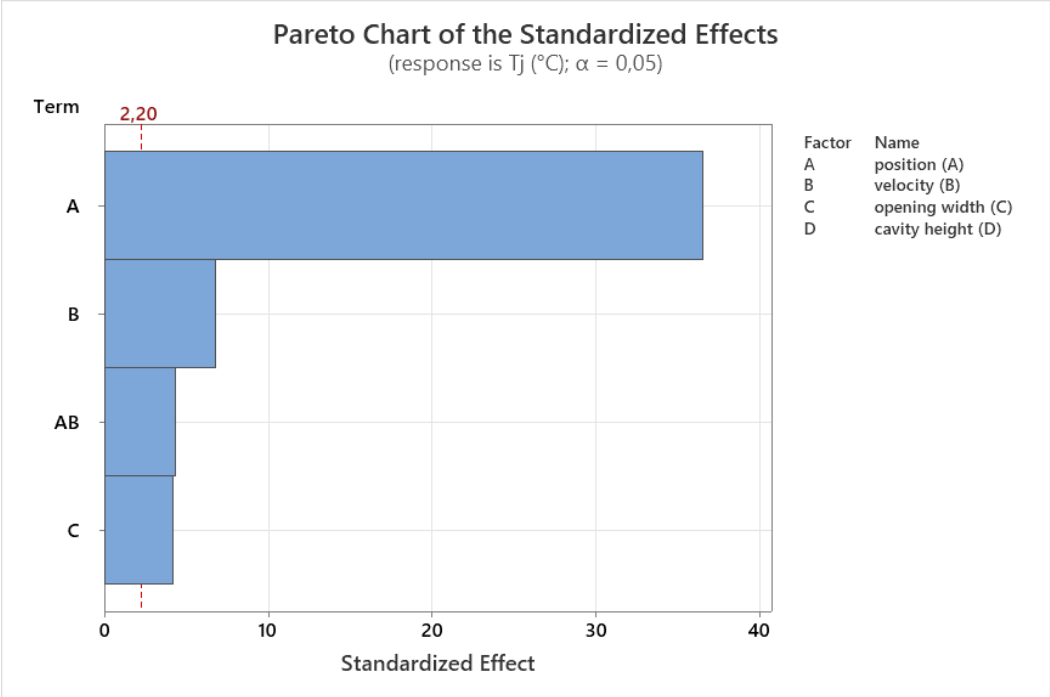

Figure 8. Pareto chart of the standardized effects for the reduced model.

Using Minitab software, this chart (Figure 8) also allows us to estimate the individual effects of these different significant parameters as well as their interactions. The amplitude

of each bar is proportional to the standardized effect, and this is equal to the estimated effect divided by its standard error. The chart in Figure 8 also contains a vertical line that corresponds to the statistical value threshold (95%). When the corresponding bar exceeds the statistical value threshold, the effect of the parameter studied is significant.

The Pareto chart shows the effects affecting the (Tj) response. We can say that the minimization of the junction temperature is directly influenced by the opening in the cavity and the addition of a well-calculated air inlet speed.

The main effects plot allows us to analyze the difference(s) between the level means of one or more factors and shows the average response for each factor level connected by a line.

Figure 9 shows the main effects of cutting parameters on temperature (Tj) as a function of cutting conditions. The analysis of the graphs shows again that the position of the opening is the most influential factor on the temperature (Tj) because it has the greatest slope, followed by the air speed and the width of the opening.

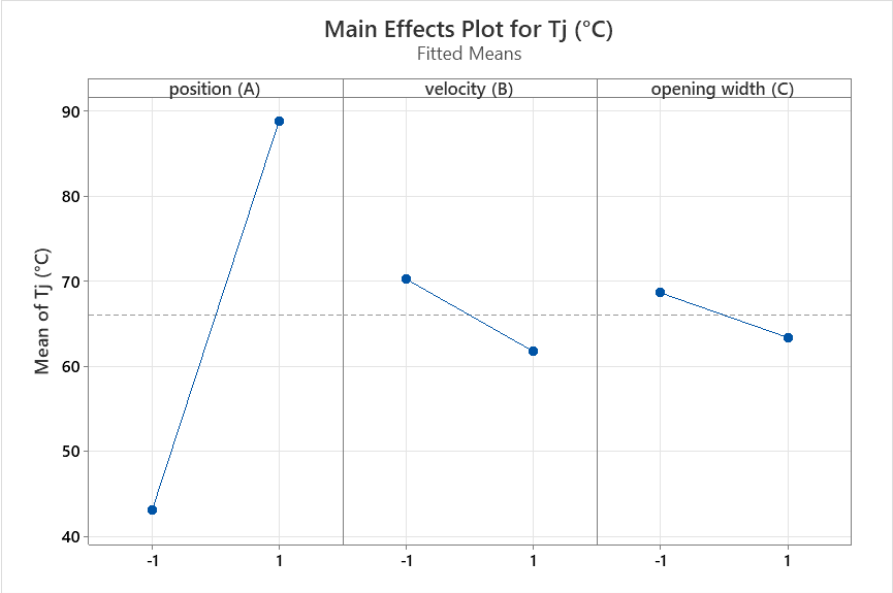

Figure 9. Main effects graph Tj (°C) for the reduced model.

5.1.3. Diagram of Interactions

Interaction plots help determine the effect of one categorical factor on the relationship between a second categorical factor and a continuous response. This graph shows the corresponding mean at one factor level on the x-axis, and a separate line for each level of the other factor.

In this interaction diagram (Figure 10), the lines are almost parallel, meaning that the interactions (A × C), (B × C) are not significant, since the different curves are almost parallel, whereas (A × B) shows a slight difference, with an interaction of 1.3%.

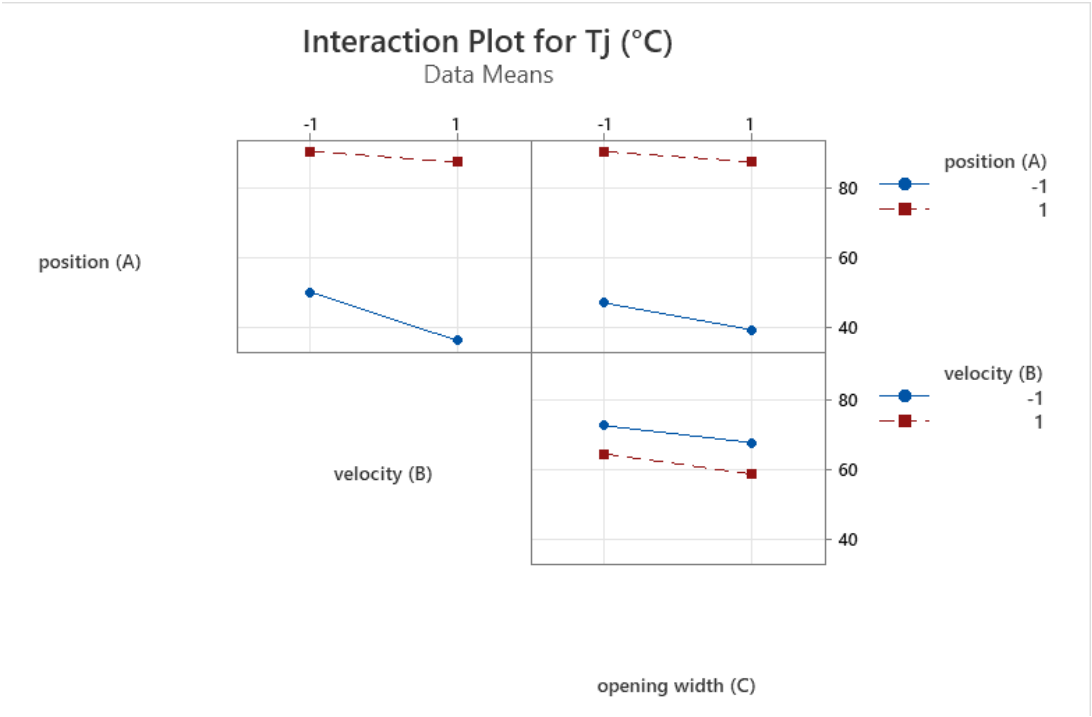

Figure 10. Interaction diagram for Tj (°C) for the reduced model.

5.1.4. Optimization and Validation of Results

In the Minitab software interface, the results optimization function allows us to mention the optimal parameters for the response according to the variables that we have entered in the worksheet of our software, as shown in Table 12.

Table 12. Optimization parameters.

Response	Objective	Target Goal	Higher Goal	Weighting	Importance
T (°C)	lower	32.86	92.72	1	1

Our goal is to minimize the junction temperature of the LED light source as much as possible. The solution is given in Table 13.

Table 13. Multiple Response Predictions Configuration.

	Variable	Configuration	
	A	-1	
	B	1	
	C	1	
	D	1	
Response	**Adjusted value**	**CI at 95%**	**IP at 95%**
Tj (°C)	31.72	(26.84; 36.61)	(24.07; 39.37)

The fitted value (also called adjusted value) for these parameters is equal to 31.72 °C. The confidence interval (CI) specifies the range of possible values for T, which, with optimization, is likely to be between 26.84 and 36.61 °C.

A prediction interval (PI) is the range likely to encompass the future response to a specified combination of variable parameters.

The desirability ranges from 1 (this is ideal) to 0 when the response is outside the acceptable range.

The optimization plot in Figure 11 shows the effects of the variables on the predicted response. This graph allows us to analytically determine the optimal values of the operating factors influencing the junction temperature using an optimization process by maximizing the desirability function.

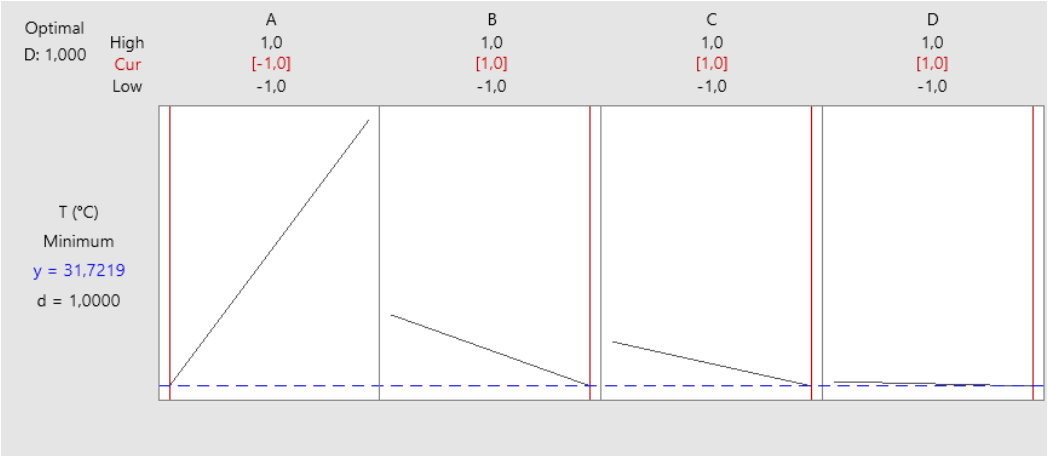

Figure 11. Response optimization.

The red vertical lines and corresponding numbers indicate the optimal factor levels, while the blue horizontal dotted line and corresponding numbers represent the average over the best factor level found. The graph indicates that when the factors are set to the values shown in red, the response T is minimized and the overall desirability value is equal to 1. From this figure, we can conclude that to obtain the lowest temperature, it suffices to use the red value, i.e., the opening in the cavity is located at 0 cm, with a width of 10cm, an air inlet speed = 2 m/s, and a height of the cavity equal to 20 cm. These parameters allow us to obtain an optimum temperature of Tj = 32.86 °C.

5.2. Thermal Analysis

A similar study was conducted in order to find correlations between the four independent factors considered in the design of experiments to calculate the convective heat transfer coefficient of the heat sink and the surrounding air.

The convective heat transfer coefficient, h_{fin} for one fin, of area A_{fin}, can be calculated:

$$h_{fin}(i) = \frac{Q_{fin}(i)}{A_{fin}\Delta T} \tag{19}$$

where $\Delta T = T_b - T_f$.

The overall heat transfer coefficient can be expressed as

$$\bar{h} = \frac{1}{N}\sum_{i=1}^{N} h_{fin}\,(i) \tag{20}$$

Figure 12 shows $\bar{h}$ as a function of time for the 16 tests carried out, corresponding to the experimental design matrix of Table 7.

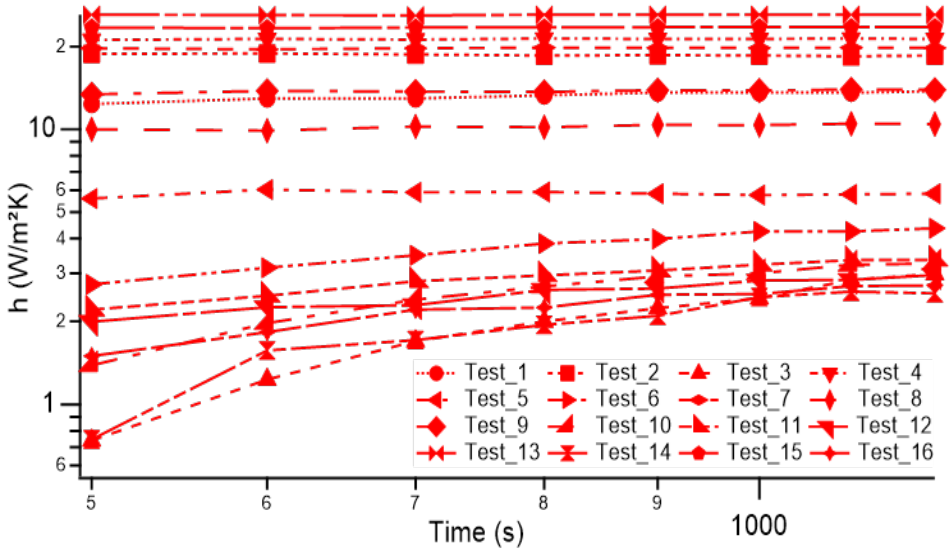

Figure 12. The convective heat transfer coefficient as a function of time for the 16 tests.

The values of $\bar{h}$ found in the steady state are then introduced into the matrix, and a correlation (Equation (21)) is deduced, for the reduced model, thus making it possible to calculate $\bar{h}$ according to the parameters A, B, and C, expressed in real values. The corresponding values of the mathematical coefficients are given in Table 14.

$$\bar{h} = h_0 + h_1 A + h_2 B + h_3 C + h_{12} A \times B \quad (21)$$

Table 14. Correlation coefficients.

h_0	h_1	h_2	h_3	h_{12}
11.150	− 7.302	2.043	0.779	− 2.185

We note that the value of the optimal coefficient corresponds to run No. 13, which corresponds to the optimal combination given in Table 13. Figure 13 represents the corresponding optimal temperature and velocity asymmetrical distributions inside the cavity. We notice the enhancement of the heat transfer convection around the heat sink thanks to the airflow coming from the hole, which justifies the maximum value of the convection heat transfer coefficient for this test. Without an opening, the air remains confined inside the cavity volume, and the thermal convection around the heat sink is mainly linked to the chimney effect of natural convection inside it (Figure 2a,b).

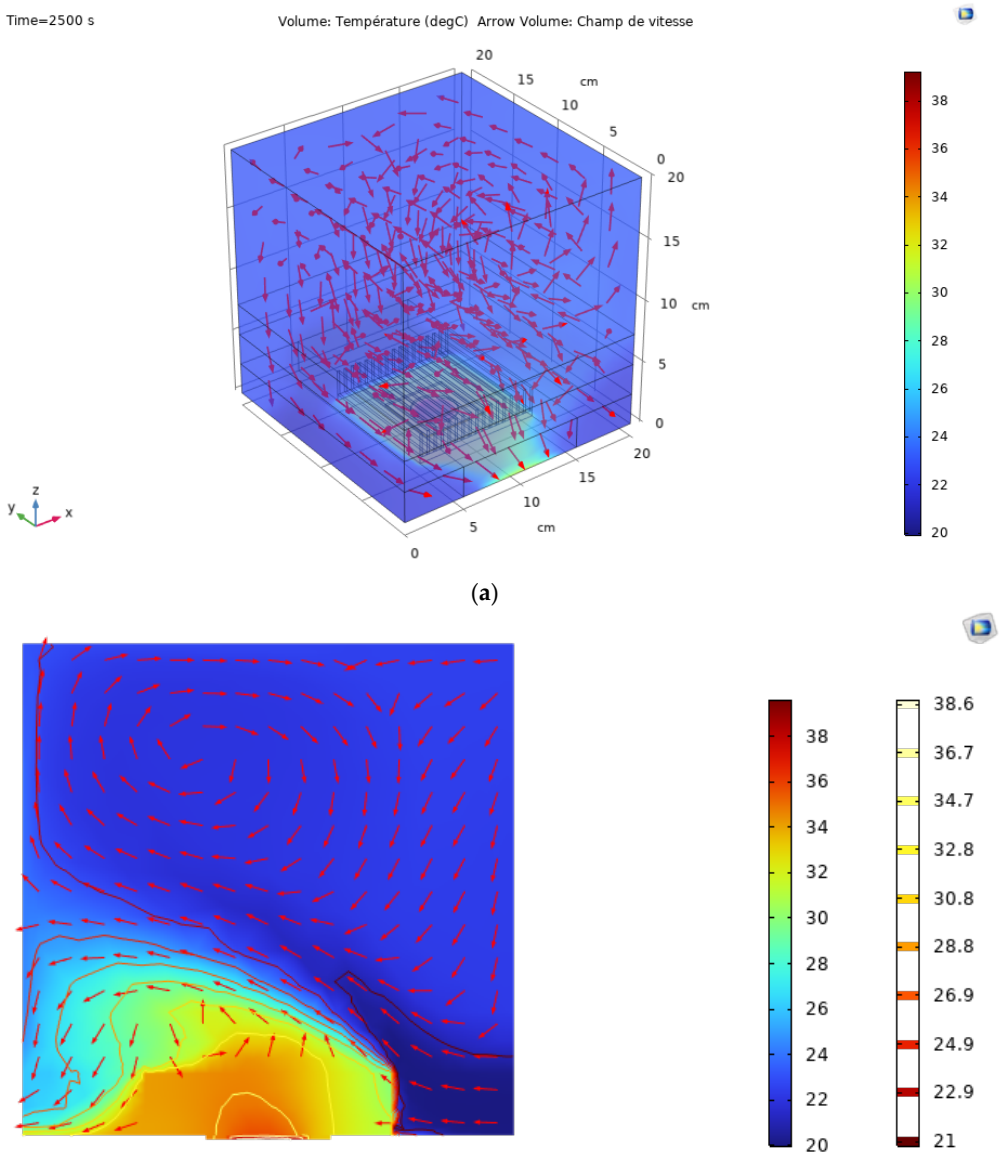

(**a**)

(**b**)

Figure 13. Asymmetrical temperature and velocity fields at t=2500 s, (a) in 3D presentation, (**b**) in 2D presentation (y-z cut-plane, x = 10 cm).

Here, an exponential model (Equation (22)) is used to predict the lifetime of the LED package.

$$L_f = \alpha \exp^{-\beta T_j} \quad (22)$$

where Tj (°C) is the junction temperature; α = 477377 and β = 0.052 [37].

Figure 14 highlights three distinct regions in the relationship between the convection coefficient (h) and the LED lifetime, each reflecting a unique thermal management behavior:

- Region 1 (h < 10 W/m²K)—Low Convection, Limited Lifetime Improvement

In this initial region, as the convection coefficient gradually increases, the LED lifetime shows only slight improvement. This behavior suggests that at low convection rates, the heat dissipation is insufficient to significantly reduce the LED's internal temperature. Consequently, the LED experiences high thermal stress, leading to slower gains in lifetime. Here, the cooling effect is limited, likely due to a boundary layer of air around the

LED that restricts heat transfer. This region could be interpreted as a baseline level of convection where gains in LED lifetime are minimal and thermal control is suboptimal.

- Region 2 (10 W/m²K ≤ h < 20 W/m²K)—Moderate Convection, Enhanced Lifetime Improvement

In this intermediate region, a notable increase in LED lifetime occurs as the convection coefficient rises. This phase indicates a transition where the heat dissipation becomes more effective, as the convection coefficient reaches a level where it can overcome the boundary layer resistance and improve cooling. As a result, the LED's temperature decreases more substantially, leading to a significant reduction in thermal stress. This region represents an optimal trade-off zone where an increase in convection has a meaningful impact on the LED's durability without reaching excessive cooling requirements.

- Region 3 (h ≥ 20 W/m²K)—High Convection, Rapid Lifetime Extension

In this final region, the LED lifetime grows exponentially with further increases in the convection coefficient. This suggests that, beyond a threshold of around 20 W/m²K, the cooling system achieves high efficiency, rapidly lowering the LED's temperature and almost eliminating thermal degradation. In this range, the system likely benefits from highly efficient heat transfer, where increased airflow or higher-quality heat sinks might be in play, providing substantial cooling that maximizes the LED's lifespan. Taking into account industrial constraints, which often consist of optimizing quality (best possible performance for heat dissipation) while reducing production costs, we have chosen convection coefficient values limited to what is strictly necessary, i.e., 15~25 W/m²K.

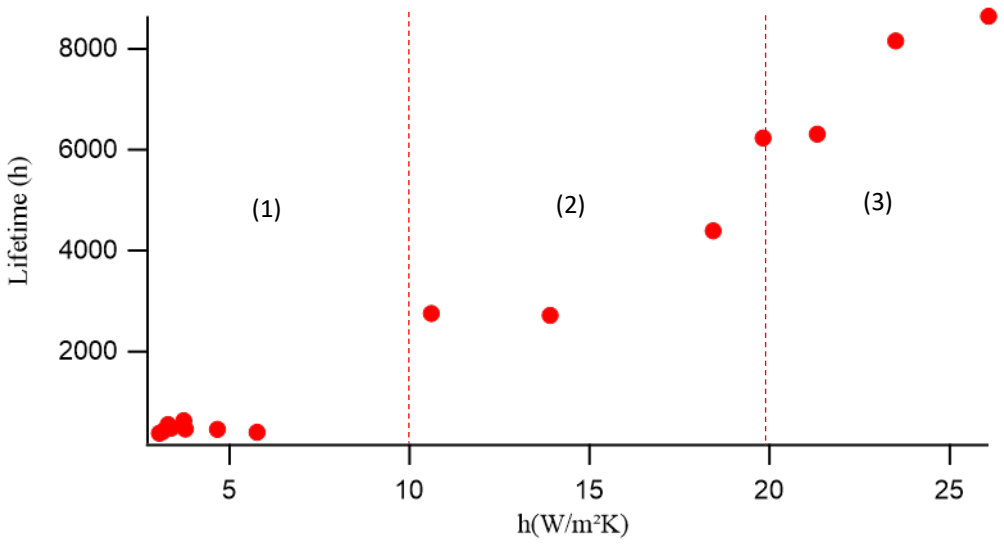

Figure 14. Relationships between the lifetime of the LED and the convection coefficient.

5.3. Effect of the Thermal Losses

In this section, we compare the effect of the different parameters studied on the junction temperature when considering different values of thermal losses.

We represent in Figure 15 the evolution of the junction temperature Tj for different percentage values, varying from $\alpha 40$ = 40% to $\alpha 70$ = 70%. It is obvious that the junction temperature is increased by decreasing the percentage of thermal losses. But this has no influence on the effects of the different factors. This is illustrated by Figure 16, which shows the effects of the different factors corresponding to the different tests according to the thermal loss percentages.

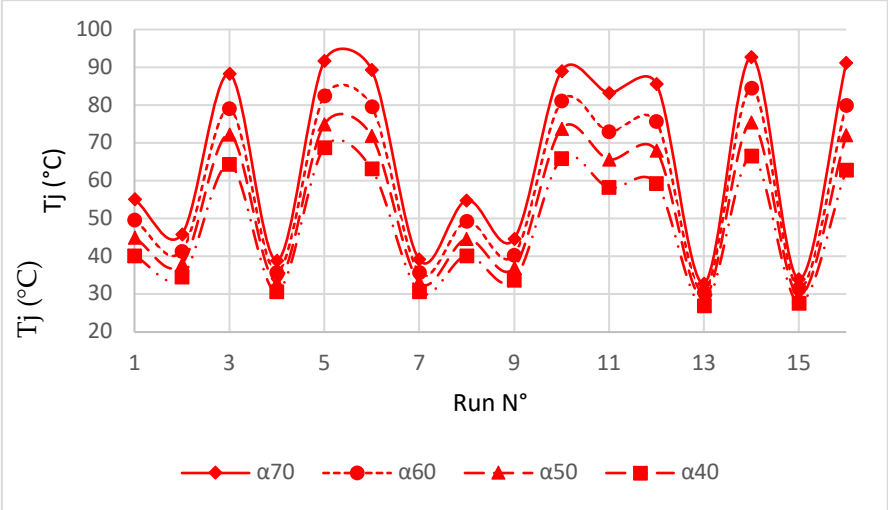

Figure 15. Evolution of the temperature for different thermal percentage values.

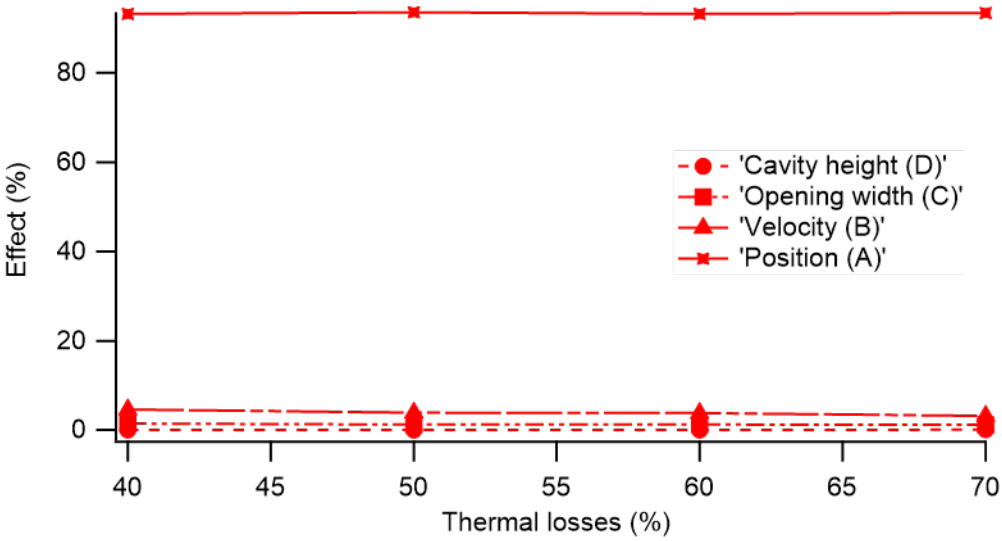

Figure 16. Effects of different parameters according to thermal percentage values.

This consistency can be explained by the fact that the geometric parameters are the primary drivers of heat dissipation. Once convection and the cavity geometry are optimized for efficient heat dissipation, variations in the amount of heat generated have little impact. In other words, these design factors play a far more significant role in thermal management than the actual amount of heat produced by the LED.

6. Conclusions

The numerical analysis treated in this paper presents results applied to the case of LED lighting sources in a confined space, such as false ceilings in interior design or the automotive field, with headlight optics. The luminous powers of LED lighting are increasingly important and are found in all possible application areas, but thermal management remains the most important point because it concerns both energy efficiency and the LED lifetime. This paper presents a typical case that can serve as a reference concerning the heat transfer by forced convection around a rectangular heat sink applied to LED lighting in a cavity with openings. An experiment and numerical modeling were carried out in order to validate our numerical model. Then, we proposed to evaluate the effects of the

position and width of the openings, the cavity height, and air velocity on the evolution of the junction temperature in order to optimize our model.

Since many input factors had to be taken into account, the following experiment design approach was used: the design of experiments was composed of four factors at two levels, which resulted in a total number of trials equal to 16. Since this number is acceptable to work with, a complete factorial design was applied.

A Pareto analysis and an analysis of variance (ANOVA) were carried out. It was found that the position of the opening is the most influential factor on the junction temperature, with a contribution of 93.46%, followed by the factors velocity and width of the opening, with low contributions (3.22% and 1.24%). We also observe that the height of the cavity is the factor that has the weakest contribution, 0.13%. These effects remain almost the same even if the thermal losses vary between 40% and 70%.

Then, a mathematical correlation was deduced to estimate the junction temperature and the convective heat coefficient of the air around the proposed heat sink and the surrounding air, depending on the three factors found to be the most significant.

Author Contributions: Conceptualization, Z.A., K.B.A., L.C., G.Z., K.C.; methodology, Z.A.; software, Z.A, K.B.A.; validation, Z.A., L.C.; formal analysis, Z.A., G.Z., K.C.; investigation, Z.A.; resources, L.C.; data curation, L.C.; writing—original draft preparation, Z.A.; writing—review and editing, Z.A., L.C.; visualization, L.C.; supervision, L.C., K.C., G.Z. All authors have read and agreed to the published version of the manuscript.

Funding: This research received no external funding.

Data Availability Statement: Data are contained within the article.

Conflicts of Interest: The authors declare no conflicts of interest.

References

1. Ishizaki, S.; Kimura, H.; Sugimoto, M. Lifetime estimation of high power white LEDs. *J. Light Vis. Environ.* **2007**, *31*, 11–18.
2. Zissis, G.; Canale, L. Éclairage à base de LEDs-Composants LED. *Opt. Photonique* **2019**, *1*, e6501.
3. Zissis, G.; Canale, L. Éclairage à base de LEDs. Conception des systems. *Tech. De L'ingénieur* **2019**, *E6502*, 23.
4. Chhajed, S.; Xi, Y.; Li, Y.-L.; Gessmann, T.; Schubert, E.F. Schubert, Influence of junction temperature on chromaticity and color-rendering properties of trichromatic white-light sources based on light-emitting diodes. *J. Appl. Phys.* **2005**, *97*, 054506.
5. Huang, B.-J.; Tang, C.-W.; Wu, M.-S. System dynamics model of high-power LED luminaire. *Appl. Therm. Eng.* **2009**, *29*, 609–616.
6. Wang, F.K.; Chu, T.P. Lifetime Predictions of LED-Based Light Bars by Accelerated Degradation Test. *Microelectron. Reliab.* **2012**, *52*, 1332–1336.
7. Wang, F.K.; Lu, Y.C. Useful Lifetime Analysis for High-Power White LEDs. *Microelectron. Reliab.* **2014**, *54*, 1307–1315.
8. Ben Abdelmlek, K.; Araoud, Z.; Ghnay, R.; Abderrazak, K.; Charrada, K.; Zissis, G. Effect of thermal conduction path deficiency on thermal properties of LEDs package. *Appl. Therm. Eng.* **2016**, *102*, 251–260.
9. Weng, C.-J. Advanced thermal enhancement and management of LED packages. *Int. Commun. Heat Mass Transf.* **2009**, *36*, 245–248.
10. Christensen, A.; Graham, S. Thermal effects in packaging high power light emitting diode arrays. *Appl. Therm. Eng.* **2009**, *29*, 364–371.
11. Heo, Y.J.; Kim, H.T.; Kim, K.J.; Nahm, S.; Yoon, Y.J.; Kim, J. Enhanced heat transfer by room temperature deposition of AlN film on aluminum for a light emitting diode package. *Appl. Therm. Eng.* **2012**, *50*, 799–804.
12. Shyu, J.-C.; Hsu, K.-W.; Yang, K.-S.; Wang, C.-C. Thermal characterization of shrouded plate fin array on an LED backlight panel. *Appl. Therm. Eng.* **2011**, *31*, 2909–2915.
13. Yu, S.-H.; Lee, K.-S.; Yook, S.-J. Natural convection around a radial heat sink. *Int. J. Heat Mass Transf.* **2010**, *53*, 2935–2938.
14. Yu, S.-H.; Lee, K.-S.; Yook, S.-J. Optimum design of a radial heat sink under natural convection. *Int. J. Heat Mass Transf.* **2011**, *54*, 2499–2505.

15. Jang, D.; Yu, S.-H.; Lee, K.-S. Multidisciplinary optimization of a pin-fin radial heat sink for LED lighting applications. *Int. J. Heat Mass Transf.* **2011**, *55*, 515–521.
16. Costa, V.A.; Lopes, A.M. Improved radial heat sink for led lamp cooling. *Appl. Therm. Eng.* **2014**, *70*, 131–138.
17. Baskaya, S.; Sivrioglu, M.; Ozek, M. Parametric study of natural convection heat transfer from horizontal rectangular fin arrays. *Int. J. Therm. Sci.* **2000**, *39*, 797–805.
18. Arularasan, R.; Velraj, R. Modeling and simulation of a parallel plate heat sink using computational fluid dynamics. *Int. J. Adv. Manuf. Technol.* **2008**, *51*, 415–419.
19. Kim, D.-K. Thermal optimization of plate-fin heat sinks with fins of variable thickness under natural convection. *Int. J. Heat Mass Transf.* **2012**, *55*, 752–761.
20. Nada, S. Natural convection heat transfer in horizontal and vertical closed narrow enclosures with heated rectangular finned base plate. *Int. J. Heat Mass Transf.* **2006**, *50*, 667–679.
21. Pathak, M.; Mer, K.; Pant, P. Numerical analysis of natural convection in rectangular enclosure with heated finned base plate. *Int. J. Res. Mech. Eng. Technol.* **2013**, *3*, 64–67.
22. Arquis, E.; Rady, M. Study of natural convection heat transfer in a finned horizontal fluid layer. *Int. J. Therm. Sci.* **2005**, *44*, 43–52.
23. Hasnaoui, M.; Vasseur, P.; Bilgen, E. Natural convection in rectangular enclosures with adiabatic fins attached on the heated wall. *Wärme-Und Stoffübertragung* **1992**, *27*, 357–368.
24. Ben Abdelmlek, K.; Araoud, Z.; Canale, L.; Ben Nejma, F.; Charrada, K.; Zissis, G. Thermal Management of LEDs Packages Within Inclined Enclosures for Lighting Applications. *IEEE Trans. Ind. Appl.* **2022**, *58*, 7998–8007. https://doi.org/10.1109/TIA.2022.3195865.
25. Smyk, E.; Gil, P.; Gałek, R.; Przeszłowski, Ł. Comparison of the Axial Fan and Synthetic Jet Cooling Systems. *Appl. Sci.* **2022**, *12*, 4349.
26. Barton, R.R. Designing Simulation Experiments. In Proceedings of the 2013 Winter Simulation Conference, 8–11 December 2013, Washington, DC, USA, 2013; Pasupathy, R.; Kim, S.-H.; Tolk, A.; Hill, R.; Kuhl, M.E., Eds.; Institute of Electrical and Electronics Engineers, Inc.: Piscataway, NJ, USA, 2013; pp. 342–353.
27. Kleijnen, J.P.C. *Design and Analysis of Simulation Experiments*; 1st ed.; Springer: New York, NY, USA, 2015.
28. Kleijnen, J.P.C.; Sanchez, S.M.; Lucas, T.W.; Cioppa, T.M. A User's Guide to the Brave New World of Designing Simulation Experiments. *Inf. J. Comput.* **2005**, *17*, 263–289.
29. Law, A.M. *Simulation and Modeling and Analysis*, 5th ed.; McGraw-Hill Education: New York, NY, USA, 2015.
30. Montgomery, D.C. *Design and Analysis of Experiments*; 8th ed.; John Wiley: New York, NY, USA, 2013.
31. Roccaforte, F.; Leszczynski, M. *Introduction to Gallium Nitride Properties and Applications*; SN-9783527347100; Wiley Online Library: Hoboken, NJ, USA, 2020; pp. 1–39. https://doi.org/10.1002/9783527825264.ch1.
32. Machado Filho, M.A.; Farmer, W.; Hsiao, C.L.; Dos Santos, R.B.; Hultman, L.; Birch, J.; Ankit, K.; Gueorguiev, G.K. Density Functional Theory-Fed Phase Field Model for Semiconductor Nanostructures: The Case of Self-Induced Core–Shell InAlN Nanorods. *Cryst. Growth Des.* **2024**, *24*, 4717.
33. Ha, M.; Graham, S. Development of a thermal resistance model for chip-onboard packaging of high power LED arrays. *Microelectron. Reliab.* **2012**, *52*, 836–844.
34. Qin, Y.X.; Hui, S.R. Comparative study on the structural designs of led devices and systems based on the general photo-electro-thermal theory. *IEEE Trans. Power Electron.* **2009**, *25*, 507–513.
35. Cengiz, C.; Azarifar, M.; Arik, M. A Critical Review on the Junction Temperature Measurement of Light Emitting lDiodes. *Micromachines* **2022**, *13*, 1615. https://doi.org/10.3390/mi13101615.
36. Baran, K.; Różowicz, A.; Wachta, H.; Różowicz, S. Modeling of Selected Lighting Parameters of LED Panel. *Energies* **2020**, *13*, 3583. 10.3390/en13143583.
37. Wang, F.K.; Chu, T.P. Lifetime predictions of LED-based light bars by accelerated degradation test. *Microelectron. Reliab.* **2012**, *52*, 1332–1336.